

Highly Sensitive and Stretchable Multidimensional Strain Sensor with Prestrained Anisotropic Metal Nanowire Percolation Networks

Kyun Kyu Kim,^{†,§} Sukjoon Hong,^{†,§} Hyun Min Cho,[†] Jinhwan Lee,[†] Young Duk Suh,[†] Jooyeon Ham,[‡] and Seung Hwan Ko^{*,†}

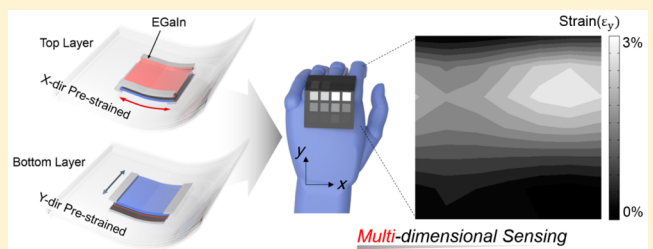
[†]Applied Nano and Thermal Science Lab, Department of Mechanical Engineering, Seoul National University, 1 Gwanak-ro, Gwanak-gu, Seoul 151-742, Korea

[‡]Department of Chemical Engineering Stanford University, 443 Via Ortega, Stanford, California 94305-4125, United States

Supporting Information

ABSTRACT: To overcome the limitation of the conventional single axis-strain sensor, we demonstrate a multidimensional strain sensor composed of two layers of prestrained silver nanowire percolation network with decoupled and polarized electrical response in principal and perpendicular directional strain. The information on strain vector is successfully measured up to 35% maximum strain with large gauge factor (>20). The potential of the proposed sensor as a versatile wearable device has been further confirmed.

KEYWORDS: multiaxis strain sensor, nanowire percolation network, stretchable electronics, anisotropic resistance change



Wearable skin-like strain sensors are becoming essential in diverse future applications, such as motion detection,^{1–11} soft robotics,^{12–15} and various biomedical applications.^{2,13,14,16–18} Among numerous nanomaterials and structures used to achieve novel flexible strain sensors, those based on carbon tend to exhibit greater mechanical performance^{3,19–22} and gains unique potential of transparency,^{4,8,23,24} but they also suffer from a low gauge factor (GF) and electrical conductivity. Similarly, sensors built with capacitive structures^{10,11,23} demonstrate excellent linearity and low hysteresis but due to the theoretical limitations, also possess poor GFs (maximum of 1). Of this latter type, sensors based on silver nanowires (Ag NWs)^{5,25–27} are suggested as the most promising candidate based on their excellent electrical and mechanical properties. However, in comparison to other recently reported silver-based strain sensors, they are only capable of detecting strain in a single direction. This hinders their application to detect more complex multiaxial, multidimensional strain conditions, with the only applicable uses being limited to areas on the body such as finger and knee joints (i.e., single axial joints). These sensors have also limited research into the quantitative determination of complex conditions in various surface strain environments. In order to obtain relevant information under such conditions, sensors need the ability to detect strain in multidimensional directions so as to emulate the strain environment. However, it is difficult to make multidimensional strain sensors because they usually show strong coupled electrical conductance change in major axis of the principal strain and perpendicular direction due to Poisson's ratio. This problem becomes more severe under large strain condition and the conventional strain sensor needs to be

exactly aligned with the principal strain to obtain accurate strain value.

To address the shortcomings of conventional single axis-strain sensor and to develop a novel scheme to detect random strain, this paper presents a highly stretchable and sensitive multidimensional strain sensor capable of detecting in real-time “skin-like” multidimensional strain loadings using prestrained Ag NW percolation networks. This relies on two prestrained percolation network layers intersecting each other, with decoupled electrical resistance change to the major axis of the principal strain and perpendicular direction and thus independently detecting the x and y axes of the surface strain environment. This sensor is demonstrated to possess excellent performance (GF ~ 20), large strain measurement (>35%), and dynamic load performance with negligible hysteresis. Moreover, very long (>80 μm) nanowire arrays are used to allow an excellent mechanical and electrical stability in percolation network and uniform output signal. The response of the sensor was theoretically studied using 3D-percolation theory, which showed excellent correspondence with the experimental signals. Computational application of the sensor to the 3D model also allowed it to be successfully operated as a multiaxial controlling device. The amplitude and angle of strain was calculated from the signal obtained from the sensor in real-time, allowing the virtual 3D model to be controlled through finger movements. The proposed Ag NW network was also applied to 4 \times 4 multipixel strain sensor array, fabricated by UV laser ablation,

Received: April 18, 2015

Revised: June 28, 2015

Published: July 7, 2015

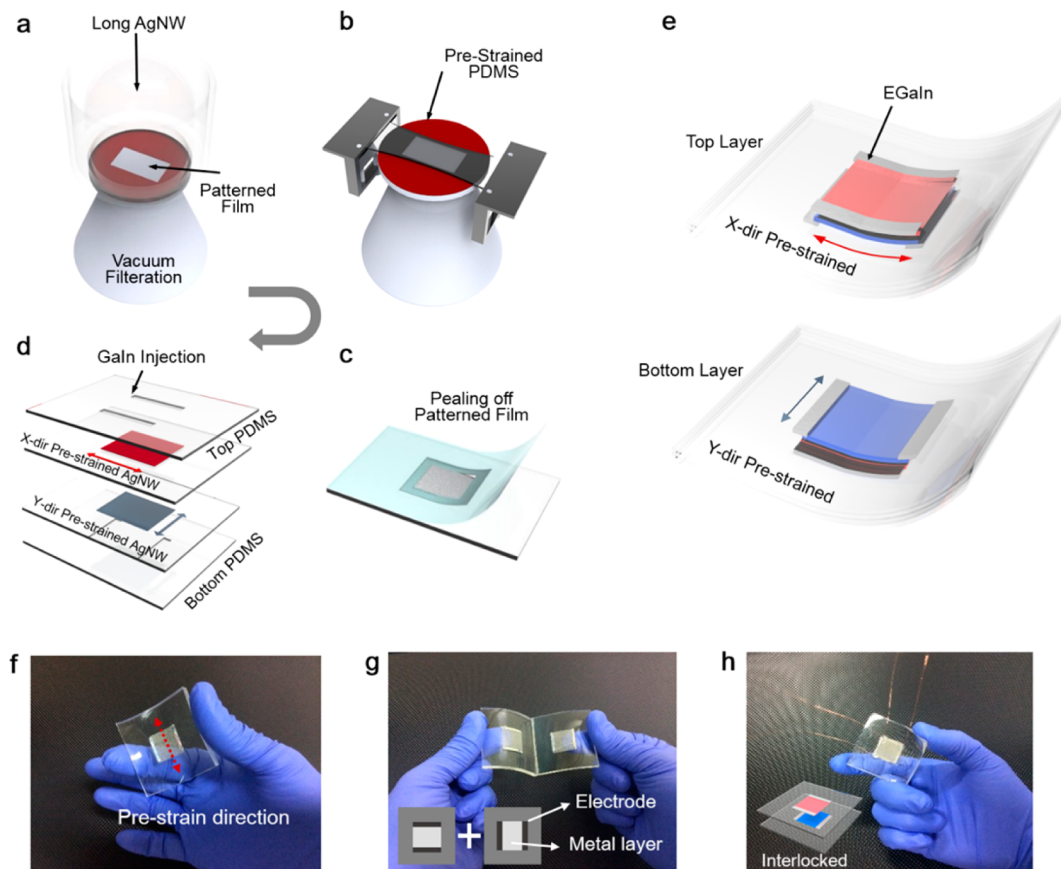


Figure 1. Fabrication of a multidimensional strain sensor. (a) Vacuum filtration and transfer of very long Ag NW percolation networks. (b) Transferring process to the prestrained PDMS substrate. (c) Edge patterning by detaching adhesive film. (d) Encapsulation of micro electrode channel and subsequent EGaIn injection. (e) Schematics showing two layers of the multidimensional strain sensor. (f) Single layer of the fabricated sensor. (g) Top and bottom layer before assembly. (h) Interlocked system of a multidimensional sensor with wire connection.

which allowed various strain conditions to be simultaneously monitored and modeled by surface strain distribution mapping.

Multidimensional strain sensor composed of prestrained Ag NW percolation network layers were prepared by vacuum filtration and transfer, as shown in Figure 1a. In this, a uniform percolation network film is first obtained by filtration of Ag NW solution, and then transferred to a prestrained (100%) PDMS substrate by applying uniform suction. The exterior of the Ag NW network is then detached and patterned by peeling off the adhesive film (Figure 1a-1c). Next, the patterned, prestrained Ag NW film is encapsulated by a PDMS micro electrode channel layer with an uncured PDMS glue layer, the latter being designed to penetrate into the pore spaces between the Ag NW interconnections. After curing to attach the encapsulation layer, all of the Ag NWs become buried between the layers to form a sandwich structure. This trilayer system is not only mechanically stable, but also resistant to surface buckling known to cause irreversibility of the resistance profile.⁵ EGaIn is then injected into this micro channel to act as a stretchable liquid electrode, as this material offers a low viscosity at room temperature and a relatively high conductivity ($\sigma = 3.4 \times 10^4 \text{ S/cm}$).^{28,29} More importantly, it maintains its fluidity after injection, which is a critical factor in establishing electrical contact between the patterned Ag NW film and the electrode during deformation of the sensor. With the help of this liquid metal channel, the entire surface of the sensor can be deformed, allowing it to be used as a nonflat surface mountable device. Finally, two of these sandwich-structured assemblies

were attached while intersecting each other (Figure 1d), with each functioning as single axis (x or y) strain sensors. The structure of the resultant multiaxial sensor is shown in Figure 1e, which is composed of two individual prestrained Ag NW strain sensors. Optical photographs of a single prestrained Ag NW strain sensor, two Ag NW sensors prestrained at perpendicular directions, and final multidimensional strain sensor after interlocking are shown in Figure 1f-1h, respectively. More detailed information on material preparation and device fabrication can be found in the Methods section.

The microscopic behavior of the surface of the prestrained Ag NW film under 100% applied strain in either the parallel (right column) or perpendicular (left column) direction with respect to the prestrain direction (central column) is shown in Figure 2a SEM pictures. Note that as the PDMS substrate shrinks to its original size after Ag NW transfer process, the surface of the Ag NW film becomes corrugated. This prestrained Ag NW percolation network film yields decoupled electrical conductance change in the applied mechanical strain direction and perpendicular direction, while the GF for conventional single axis strain sensors show highly coupled electrical conductance change due to Poisson's ratio. The physical phenomenon behind the polarized and decoupled resistance change in perpendicular direction and parallel direction (Figure 2b) can be explained by these surface conditions. The strain applied to the prestrained direction (Figure 2a, right inset, "parallel direction") caused the surface to become unwrinkled, yet still maintain its percolation

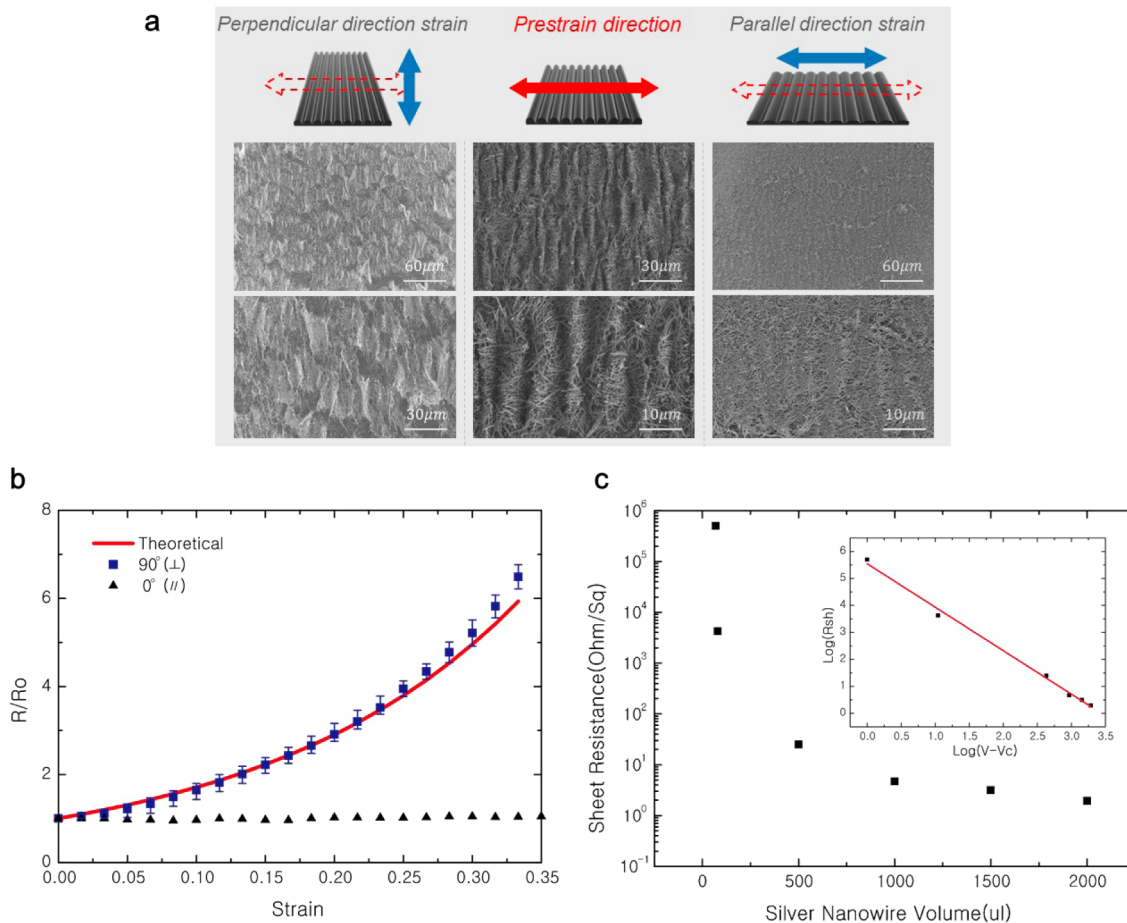


Figure 2. Decoupled and polarized response of the Ag NW network strain sensor. (a) SEM image showing the surface of the sensor when strain is applied in the perpendicular (right column) and parallel direction (left column). (b) Variation in resistance for parallel (0°) and perpendicular (90°) directional deformation in comparison with the theoretical value derived by 3D percolation theory. (c) Sheet resistance as a function of the volume of silver nanowires. The inset shows a logarithmic plot of the data with a linear fit.

network and electrical conductance until it reaches the prestrain value. This made possible by the fact that Ag NWs are very ductile and malleable, and therefore capable of enduring a large degree of strain and deformation.³⁰ Since the corrugated surface is structurally flattened along the parallel to the prestrain direction (Figure 2a, right inset, “parallel direction”), a resistance shows almost no change up to certain strain. In contrast, the strain applied to the perpendicular to the prestrain direction (Figure 2a, left inset, “perpendicular direction”) causes the distance between nanowires to increase, deforming them in the strain direction while maintaining their wavy surface in parallel direction. Since the Ag NWs used in this study is much longer ($>80 \mu\text{m}$) than typical Ag nanowires ($1-20 \mu\text{m}$),³³ it is possible to make more effective use of the percolation network with greater stretchability³⁰⁻³² and stability of the resistance profile under the strain in any direction.

As shown in Figure 2b, a strain applied at 0° (triangle symbol, parallel to the prestrained direction) generates almost no resistance variation, while a 90° strain (square symbol, perpendicular to the prestrained direction) generates a dramatic increase in resistance. In other words, the proposed prestrained strain sensor shows polarized and decoupled resistance change to a principal strain axis and therefore displays a sinusoidal response to off-axis strain angles (see Supporting Information video clip 1). As a result, the two crossing strain sensors are

capable of independently detecting the transverse and longitudinal axes strain. This trend has been maintained at least up to 35% strain, while the limit of detection³⁴ toward the perpendicular direction is measured to be as small as 0.5%.

Physical analysis of the proposed Ag NW percolation network strain sensor was carried out using 3D percolation theory $\sigma = \sigma_0(V - V_c)^\alpha$, where σ_0 is the electrical conductivity of the Ag NWs ($630,000 \text{ S/cm}$), σ is the electrical conductivity of the Ag NW network, V is the volumetric fraction of Ag NWs in the filler (PDMS), V_c is the volumetric fraction of Ag NW at the percolation threshold, and α is the critical fitting exponent. Figure 2c shows the change in sheet resistance with nanowire volume, being measured by a four-point method after transferring the metal layer to the glass substrate. For the given nanowire concentration of 0.1 mg/mL (ethanol based) used in this study, the percolation threshold was calculated as a surface concentration of $7.276 \mu\text{L}/\text{cm}^2$, the validity of which was confirmed through Monte Carlo simulation (Supporting Information (Figure S4)). This percolation threshold represents the minimum amount of Ag NWs required to ensure a successive percolation network to achieve a conductive film. The best fitting line was obtained by taking a value of $\alpha = 1.612$, which corresponds to the inclination of the fitted line of the $\log(R_{sh})$ vs $\log(V - V_c)$ graph (Figure 2c, inset). As strain is applied, the volume of filler (V_{pdms}) is increased, whereas the volume of AgNW (V_{AgNW}) remains the same. Consequently,

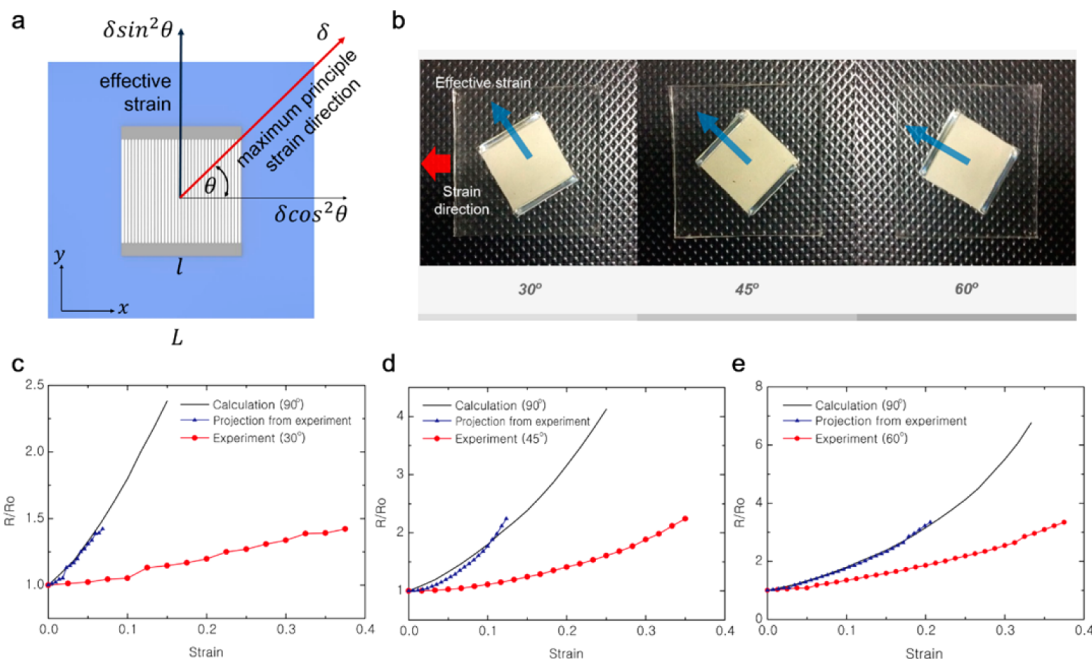


Figure 3. Detecting off-axis principal strain. (a) Schematic of the strain components applied to the strain sensor. (b) Photographs of the metal layer rotated to different angles. (c–e) Comparison of the variation in resistance of the rotated sensor with that of the sensor strained at 90°. Blue triangle lines shows the projected strain value for 90° from experiment data for each off-axis rotation.

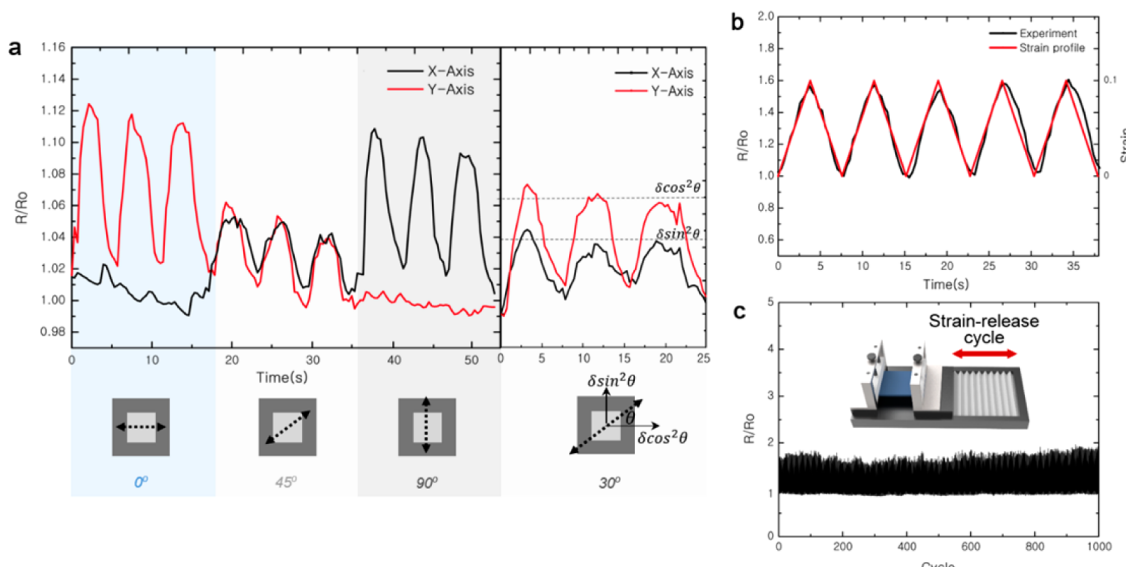


Figure 4. Cyclic response of the proposed strain sensor. (a) Real-time monitoring of load-unload strain cycles at various off-axis strain angles (0°, 45°, 90°, 30°). (b) Response of a strain sensor under the prescribed dynamic strain profile. (c) Long-term cyclic strain response test (1000 cycles).

the volumetric fraction of V ($V_{\text{AgNW}}/V_{\text{pdms}}$) decreases with increasing strain, leading to a decrease in conductivity (see Supporting Information for details). Using these obtained values, the theoretical variation in resistivity was successfully calculated and found to match well with the experimental values given in Figure 2b (red line). Furthermore, the initial resistance of the strain sensor (5.3Ω) increased significantly to 36Ω , which is nearly seven times larger than the initial resistivity when a 35% strain was applied.

In order to demonstrate the proposed sensor's ability to detect multidimensional strain, the results obtained by the experiment shown in Figure 3 were compared with theoretical calculations (black lines in Figure 3c–e). The resistance of the

Ag NW percolation network film pretrained in the x direction (parallel to the pretrained direction) is affected by the strain applied in the y direction (perpendicular to the pretrained direction). Therefore, if there is a strain δ applied in the off-axis direction (maximum principal strain direction, θ degree rotated from the pretrained direction), the deformation affecting electrical conductivity will be $\delta \sin^2 \theta$. Owing to the inherent limitations of a single-axial tensile testing stage, applying a uniform axial strain in a specific off-axis direction is the most challenging technique in the aspects of theoretical and quantitative analysis. This problem was therefore approached by simply rotating the metal layer during the transfer process rather than vary the axial direction of strain, as depicted in

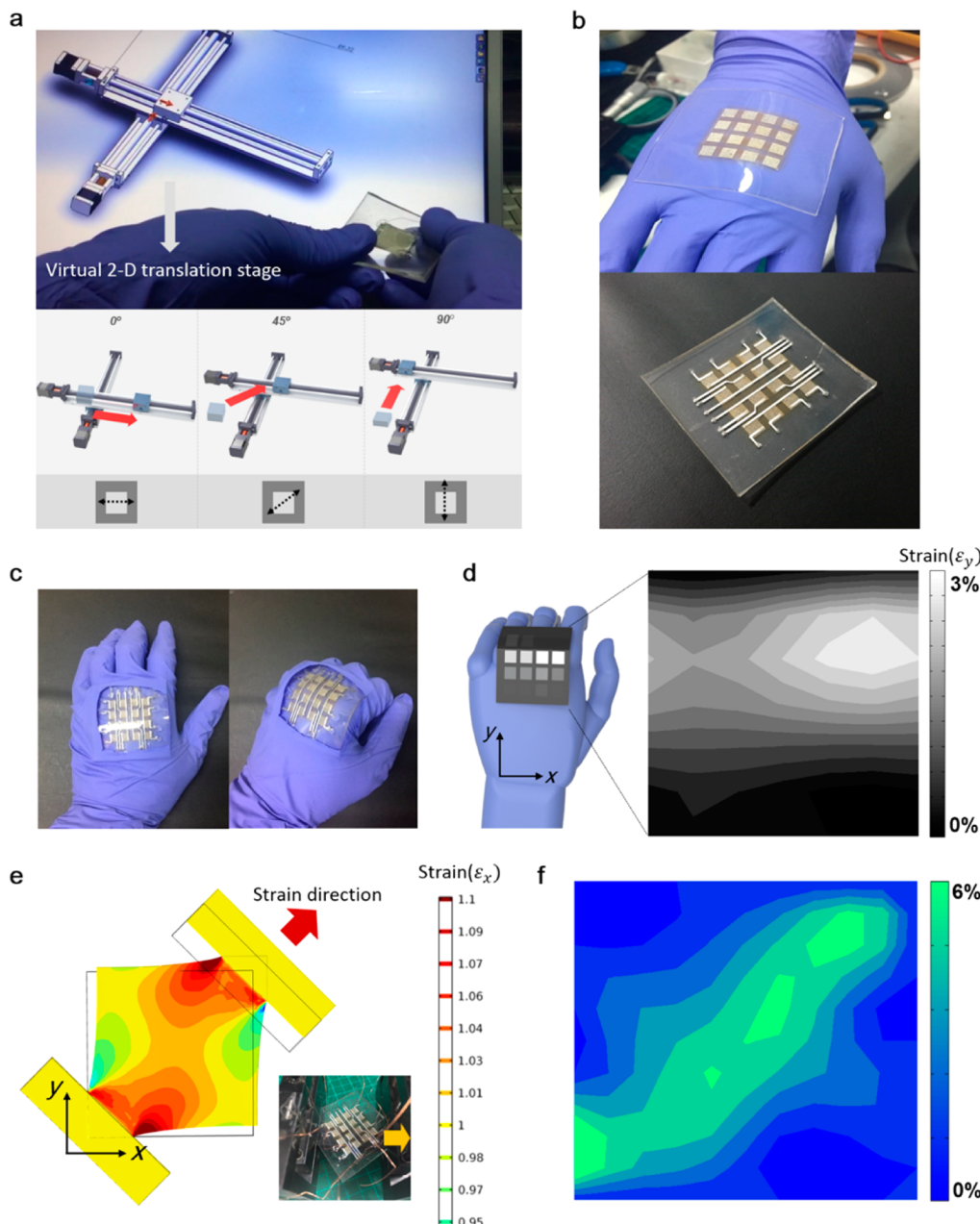


Figure 5. Demonstration of applications of multidimensional strain sensors. (a) Control of a virtual 3D translation stage using a multidimensional strain sensor. (b) Photograph of a multipixel strain sensor array. (c) Photograph of the sensor embedded in a glove to provide hand grip motion. (d) Mapping of the strain distribution for hand grip motion in (c). (e) FEA simulation of 45° elongation and a strain distribution of ϵ_x . (f) Experimental mapping of the ϵ_x strain distribution for random directions of strain loading. Experimental results show good agreement with FEA simulation in (e).

Figure 3b (where the direction of strain is maintained along the x axis). The effective strain factor in this case is determined as $\cos \theta / (1 + \tan \theta)$ (See Supporting Information Figure S3) and makes it possible to calculate the effective strain by simply multiplying to the original strain value. This, in turn, allows the amplitude of the resistance to be predicted for various strain directions, as shown in Figure 3c–e (blue triangles, “projected from experiments”). A single Ag NW percolation network layered sensor was deformed in a tensile testing stage while measuring the minute resistance variation at 1.25% strain intervals. As mentioned earlier, the response output of the sensor increases with off-axis angle (90°, perpendicular to the prestrained direction) and by multiplying the factors at 60°, 45°, and 30° (0.549, 0.353, 0.183, respectively) with their

corresponding strain values, the effective strain is found to match perfectly with the original resistance profile at 90° strain angle deformation (black lines). This successfully demonstrates the accurate performance of the strain sensor, and from the information above, it is possible to calculate and predict the resistance responses on arbitrary strain directions and strain values. Moreover, one can inversely calculate both the magnitude of the maximum principal strain and its direction from the measured change in resistance by using two perpendicular strain sensors, as these independently detect the perpendicular axes of the maximum principal strain.

The response of the strain sensor under cyclic strain (Figure 4a) were recorded in various off-axis strain directions by applying minute manual deformation with fingers. The black

line represents the x -axis prestrained sensor, while the red line is the y -axis prestrained sensor. As can be seen in the figure (Figure 4a), an erratic movement of the finger was precisely and instantaneously recorded on the output signal. Under the off-axis strain at 0° , the y -axis prestrained sensor (red line) shows substantial response, whereas the x -axis prestrained sensor (black line) does not react to the strain signal. At 45° , however, both x - and y -axis sensors show identical output signals, whereas at 90° , the variation is opposite to that observed at 0° .

The maximum principal strain (amplitude and direction of maximum principal strain) can be theoretically calculated using the schematic illustrated in Figure 3a. If we assume that there is a strain δ applied in the off-axis (θ) direction, then the strain on each axis can be expressed as $\delta_x = \delta \cos^2 \theta$ and $\delta_y = \delta \sin^2 \theta$ for the x axis and y axis, respectively. The strain direction of the sensor can be expressed as $\theta = \tan^{-1}(\delta_y/\delta_x)^{1/2}$, and the amplitude of the maximum principle strain can be further expressed as $\epsilon = \delta_x/\cos^2 \theta$ or either as $\epsilon = \delta_y/\sin^2 \theta$. Thus, the direction of the maximum principal strain can be easily calculated by analyzing the amplitude ratio of the two sensors' output. For example, with 45° strain applied, the ratio between δ_x and δ_y is one, which explains the identical strain variation observed (see Supporting Information video clip 2).

To measure the accuracy and response time of Ag NW percolation network strain sensor, a linear actuator system was used to apply dynamic cyclic strain (10%). The output signals recorded from the sensor are given in Figure 4b and show excellent agreement with the resistance profile theoretically calculated from Figure 2b. Figure 4c shows the long-term reliability of the sensor. Signals collected after 1000 cycles showed that there is negligible change in the resistance profile with repeated loading.

The multidimensional strain sensors can be used as an input device of a maximum principal strain information. A virtual 3D simulation model of a multiaxis translation stages was connected to the multidimensional Ag NW percolation network strain sensor and its movement was controlled by the strain sensor signal with communication provided through a homemade data acquisition system linked to a 3D CAD program. This allowed the model to be successfully controlled by a finger in the 0° , 45° , and 90° directions, as shown in Figure 5a.

Another advantage of Ag NW based strain sensor is that its patterning can be conducted very easily. Through a simple patterning process, Ag NW percolation network enables spatial mapping of strain. A multipixel strain senor array of 16 (4×4) is fabricated by UV laser ablation patterning of the Ag NW percolation network for simultaneous measurement of the spatial strain distribution. As an application, strain distribution of the hand grip is monitored by the fabricated multipixel strain sensor. The human hand is a very complex organ capable of many different motions and fine motor skills. Therefore, it is extremely difficult to anticipate complete hand motion by simply measuring its 2D strain state. Hence, we concentrate on one of its representative motions—hand grip—which largely involves strain in the y direction. In this purpose, other strain, such as abduction and adduction in x direction, affects the measurement as accumulating unwanted signals. Therefore, Ag NW percolation network prestrained in the x direction has been used to exclude the strain components in the x direction that are irrelevant to our purpose. A PDMS microelectrode array was subsequently encapsulated above the metal layer

pixels with following process of EGaIn injection, as demonstrated in Figure 5b. The photograph of the resultant sensor embedded in a glove for the measurement is provided in Figure 5c. In the strain distribution map provided in Figure 5d, the brighter spot corresponds to a region of greater elongation. It is noticeable that the maximum strain is detected at the joint as anticipated. To further explore the sensor's ability to detect random directional loadings, a 5% strain was applied in the 45° direction to the multipixel strain sensor. The experimental settings were identical to those modeled in the finite element analysis (FEA) simulation (calculated strain distribution through FEA in the x direction (ϵ_x) are shown in Figure 5e). As evidenced by the experimental results in strain mappings (Figure 5f), the sensor is perfectly capable of distinguishing and detecting strain distribution on the surface, showing excellent agreement with the strain distribution modeled by FEA simulation.

In summary, we have presented a highly sensitive, flexible, and stable multidimensional strain sensor that could be applied to next-generation multidimensional electronic sensing devices. This sensor consists of a prestrained metal nanowire percolation network created through a simple fabrication method with the very long nanowires that greatly enhance the electrical performance of the sensor. The proposed metal nanowire wire percolation network strain sensor showed highly polarized and decoupled electrical resistance change in the axial direction and perpendicular direction and could measure the maximum principal strain. Experimentally obtained properties of the resultant strain sensor in terms of large GF (~20) and large stretchability (35%) show its potential to detect any kind of natural strain where a large strain and sensitivity are required. Furthermore, as the sensor is applicable to both 2-dimensional controlling devices and areal strain detection, it may have a large impact in the implementation of future wearable device that often requires both monitoring and controlling of various surface conditions in human skin, mechanical structures, and soft robotics.

Methods. *Very Long Ag NW Synthesis.* The modified polyol method^{35,36} was used to synthesize very long AgNWs: 0.234 g of PVP ($M_w \sim 360\,000$) was added to 50 mL of EG and dissolved by using a magnetic stir at 150 °C. Afterward, a Cu additive ($CuCl_2$) solution was dumped to PVP solution. After 5–10 min, 15 mL of a 94 mM $AgNO_3$ solution were injected sequentially. The reaction condition was maintained until the synthesis was completed. The synthesized AgNWs were cleaned with acetone and ethanol at a 10:1 v/v ratio three times and collected by centrifugation of 3000 rpm for 20 min.

Fabrication of the Strain Sensor. Prestrained AgNW films were prepared by pouring a 0.01 wt % AgNW solution dispersed in ethanol through a 0.2 μm porous membrane filter (diameter = 49 mm). Any ethanol remaining on the filter was gently dried by an air blower, after which the target prestrained substrate (PDMS) was placed on top of the filter. A uniform vacuum pressure was applied to transfer the AgNW layer on to the target substrate, and then the membrane was peeled off to leave the AgNW layer on the prestrained substrate. This prestrained substrate then steadily returned to its original nonstrained condition.

Patterns of micro electrode channels on the cover layer were defined by photolithography. PDMS (Dow Corning, Sylgard 184) was poured on the wafer with SU-8 patterned master wafer and fully curing it in an oven at 100 °C for 20 min. After peeling the cured PDMS from the wafer, channels measuring

250 μm in height were obtained (the fabrication of SU-8 master mold can be also replaced with the simple maskless fabrication shown in Supporting Information Figure S6). A PDMS glue layer was then spin coated onto the bottom of this cover layer and partially cured in an oven at 50 °C for 30 min. Next, the partially cured cover layer was attached to the prestrained AgNW film layer and fully cured in an oven at 100 °C for 10 min. After injecting EGaIn (Aldrich) into the channel by applying a positive pressure with a syringe, a single copper wire was inserted into the EGaIn-filled micro electrode channel to transfer current and enable resistance measurement. The resulting channels therefore act as a stretchable and flexible electrode.

■ ASSOCIATED CONTENT

Supporting Information

Calculation of resistance through 3D percolation theory, AFM and SEM images, resistance values, calculation of the effective strain for off-axis deformation figure, Monte Carlo simulation of resistance through 3D percolation theory, length characterization of the synthesized long Ag NWs, multipixel strain sensor fabrication, video clip of output signals of single axial prestrained sensor under x - and y -bending cycles, video clip of controlling virtual translation stage with 2-D strain sensor. The Supporting Information is available free of charge on the ACS Publications website at DOI: 10.1021/acs.nanolett.5b01505.

■ AUTHOR INFORMATION

Corresponding Author

*E-mail: maxko@snu.ac.kr.

Author Contributions

[§]Kyun Kyu Kim and Sukjoon Hong contributed equally to this work.

Notes

The authors declare no competing financial interest.

■ ACKNOWLEDGMENTS

This work is supported by National Research Foundation of Korea (NRF) (grant no. 2012-0008779) Global Frontier R&D Program on Center for Multiscale Energy System (grant no. 2012-054172) funded by the Ministry of Science, ICT & Future, and the R&D Convergence Program, and by Seoul National University, Institute of Advanced Machinery and Design (SNU-IAMD).

■ REFERENCES

- (1) Pang, C.; et al. A flexible and highly sensitive strain-gauge sensor using reversible interlocking of nanofibres. *Nat. Mater.* **2012**, *11*, 795–801.
- (2) Park, J.; et al. Giant tunneling piezoresistance of composite elastomers with interlocked microdome arrays for ultrasensitive and multimodal electronic skins. *ACS Nano* **2014**, *8*, 4689–4697.
- (3) Cohen, D. J.; Mitra, D.; Peterson, K.; Maharbiz, M. M. A highly elastic, capacitive strain gauge based on percolating nanotube networks. *Nano Lett.* **2012**, *12*, 1821–1825.
- (4) Cai, L.; et al. Super-stretchable, transparent carbon nanotube-based capacitive strain sensors for human motion detection. *Sci. Rep.* **2013**, *3*, 3048.
- (5) Amjadi, M.; Pichitpongkit, A.; Lee, S.; Ryu, S.; Park, I. Highly stretchable and sensitive strain sensor based on silver nanowire-elastomer nanocomposite. *ACS Nano* **2014**, *8*, 5154–5163.
- (6) Lessing, J.; Morin, S. A.; Keplinger, C.; Tayi, A. S.; Whitesides, G. M. Stretchable Conductive Composites Based on Metal Wools for Use as Electrical Vias in Soft Devices. *Adv. Funct. Mater.* **2015**, *25*, n/a–n/a.
- (7) Li, X.; et al. Stretchable and highly sensitive graphene-on-polymer strain sensors. *Sci. Rep.* **2012**, *2*, 870.
- (8) Lipomi, D. J.; et al. Skin-like pressure and strain sensors based on transparent elastic films of carbon nanotubes. *Nat. Nanotechnol.* **2011**, *6*, 788–792.
- (9) Muth, J. T.; et al. Embedded 3D printing of strain sensors within highly stretchable elastomers. *Adv. Mater.* **2014**, *26*, 6307–6312.
- (10) Viry, L.; et al. Flexible three-axial force sensor for soft and highly sensitive artificial touch. *Adv. Mater.* **2014**, *26*, 2659–2664.
- (11) Woo, S.-J.; Kong, J.-H.; Kim, D.-G.; Kim, J.-M. A thin all-elastomeric capacitive pressure sensor array based on micro-contact printed elastic conductors. *J. Mater. Chem. C* **2014**, *2*, 4415.
- (12) Ma, R.; Lee, J.; Choi, D.; Moon, H.; Baik, S. Knitted fabrics made from highly conductive stretchable fibers. *Nano Lett.* **2014**, *14*, 1944–1951.
- (13) Kim, J.; et al. Stretchable silicon nanoribbon electronics for skin prosthesis. *Nat. Commun.* **2014**, *5*, 5747.
- (14) Lu, N.; Lu, C.; Yang, S.; Rogers, J. Highly Sensitive Skin-Mountable Strain Gauges Based Entirely on Elastomers. *Adv. Funct. Mater.* **2012**, *22*, 4044–4050.
- (15) Cheng, M.; Huang, X.; Ma, C.; Yang, Y. A flexible capacitive tactile sensing array with floating electrodes. *J. Micromech. Microeng.* **2009**, *19*, 115001.
- (16) Huang, X.; et al. Materials and Designs for Wireless Epidermal Sensors of Hydration and Strain. *Adv. Funct. Mater.* **2014**, *24*, 3846–3854.
- (17) Kang, D.; et al. Ultrasensitive mechanical crack-based sensor inspired by the spider sensory system. *Nature* **2014**, *516*, 222–226.
- (18) Pang, C.; et al. Highly skin-conformal microhairy sensor for pulse signal amplification. *Adv. Mater.* **2015**, *27*, 634–640.
- (19) Alamusi, H.; Fukunaga, H.; Atobe, S.; Liu, Y.; Li, J. Piezoresistive strain sensors made from carbon nanotubes based polymer nanocomposites. *Sensors* **2011**, *11*, 10691–10723.
- (20) Hu, N.; et al. Investigation on sensitivity of a polymer/carbon nanotube composite strain sensor. *Carbon* **2010**, *48*, 680–687.
- (21) Yamada, T.; et al. A stretchable carbon nanotube strain sensor for human-motion detection. *Nat. Nanotechnol.* **2011**, *6*, 296–301.
- (22) Kang, I.; Schulz, M. J.; Kim, J. H.; Shanov, V.; Shi, D. A carbon nanotube strain sensor for structural health monitoring. *Smart Mater. Struct.* **2006**, *15*, 737.
- (23) Wang, X.; Li, T.; Adams, J.; Yang, J. Transparent, stretchable, carbon-nanotube-inlaid conductors enabled by standard replication technology for capacitive pressure, strain and touch sensors. *J. Mater. Chem. A* **2013**, *1*, 3580.
- (24) Bae, S.-H.; Lee, Y.; Sharma, B. K.; Lee, H.-J.; Kim, J.-H.; Ahn, J.-H. Graphene-based transparent strain sensor. *Carbon* **2013**, *51*, 236–242.
- (25) Yao, S.; Zhu, Y. Wearable multifunctional sensors using printed stretchable conductors made of silver nanowires. *Nanoscale* **2014**, *6*, 2345–2352.
- (26) Xu, F.; Zhu, Y. Highly conductive and stretchable silver nanowire conductors. *Adv. Mater.* **2012**, *24*, 5117–5122.
- (27) Yun, S.; Niu, X.; Yu, Z.; Hu, W.; Brochu, P.; Pei, Q. Compliant Silver Nanowire-Polymer Composite Electrodes for Bistable Large Strain Actuation. *Adv. Mater.* **2012**, *24*, 1321–1327.
- (28) Dickey, M. D.; Chiechi, R. C.; Larsen, R. J.; Weiss, E. A.; Weitz, D. A.; Whitesides, G. M. Eutectic Gallium-Indium (EGaIn): A Liquid Metal Alloy for the Formation of Stable Structures in Microchannels at Room Temperature. *Adv. Funct. Mater.* **2008**, *18*, 1097–1104.
- (29) Kubo, M.; et al. Stretchable microfluidic radiofrequency antennas. *Adv. Mater.* **2010**, *22*, 2749–2752.
- (30) Lee, P.; et al. Highly stretchable and highly conductive metal electrode by very long metal nanowire percolation network. *Adv. Mater.* **2012**, *24*, 3326–3332.
- (31) Lee, J.; et al. Very Long Ag Nanowire Synthesis and Its Application for a Highly Transparent, Conductive and Flexible Metal Electrode Touch Panel. *Nanoscale* **2012**, *4*, 6408–6414.

- (32) Lee, J.; et al. Large-scale Synthesis and Characterization of Very Long Silver Nanowires via Successive Multistep Growth. *Cryst. Growth Des.* **2012**, *12*, 5598–5605.
- (33) Kumar, A.; Zhou, C. The race to replace tin-doped indium oxide: which material will win? *ACS Nano* **2010**, *4*, 11–14.
- (34) Currie, L. A. Limits for qualitative detection and quantitative determination. Application to radiochemistry. *Anal. Chem.* **1968**, *40*, 586–593.
- (35) Lee, J.; et al. Room-Temperature Nanosoldering of a Very Long Metal Nanowire Network by Conducting-Polymer-Assisted Joining for a Flexible Touch-Panel Application. *Adv. Funct. Mater.* **2013**, *23*, 4171–4176.
- (36) Lee, P.; et al. Highly stretchable or transparent conductor fabrication by hierarchical multiscale hybrid nanocomposite. *Adv. Funct. Mater.* **2014**, *24*, 5671–5678.